

Cluster surface states for TiO_2 , SrTiO_3 , and BaTiO_3

T. Wolfram and R. Hurst

Department of Physics, University of Missouri-Columbia, Columbia, Missouri 65201

F. J. Morin

Science Center, Rockwell International, Thousand Oaks, California 91360

(Received 10 February 1976)

The properties of cluster surface states of the transition-metal oxides TiO_2 , SrTiO_3 , and BaTiO_3 are derived from an empirical molecular-orbital model. The relation between cluster states and bulk and surface energy bands is discussed. The possible role of surface states in producing the 2.0-eV peak observed in the electron energy-loss spectrum of TiO_2 and Ti_2O_3 is suggested. Some comments on the use of a cluster model for the interpretation of optical properties are also included.

I. INTRODUCTION

In previous works¹⁻³ we have discussed the electronic properties of bulk and surface energy bands of d -band perovskites such as SrTiO_3 , BaTiO_3 , or KTaO_3 . An important result of these studies is the prediction of highly localized conduction and valence surface bands with energies in the forbidden energy gap. It was shown that the surface conduction bands produce a high density of d -electron states involving the t_{2g} -symmetry d orbitals.³ In pure-insulating perovskites the d -electron states are empty. They may be populated by reduction of the material or by the action of band-gap light.

The d -electron surface states have the proper symmetry and energies for interaction with the antibonding orbitals of many diatomic molecules and dissociative chemisorption of molecular hydrogen or oxygen on the surface of a perovskite is likely to be initiated by transfer of electrons from an occupied surface state into the empty molecular antibonding states. It is also believed that the d -electron surface states are effective in catalyzing alkene addition at a C=C bond by interaction with the π electrons to lower the activation energy. A conceptual model for cyclobutanation of ethylene involving the d -electron surface states has been recently discussed by Wolfram and Morin.⁴

In this paper we present a simple molecular-orbital model for the MO_6 cluster states of a transition-metal ion (M) surrounded by an octahedron of oxygen ions. Cluster-state analogs of the surface energy bands are produced when the environment of one of the oxygens is perturbed or when one of the oxygen ions is missing, as can occur at the surface of a solid. The qualitative features of such cluster surface states are discussed and compared with those of the corresponding surface energy bands. Numerical results ap-

plicable to TiO_2 , SrTiO_3 , and BaTiO_3 are presented. We also present a calculation of the surface energy bands derived from the d orbitals of e_g symmetry.

A comparison of cluster- and band-theory surface states is of interest for several reasons. In the case of strong chemisorption on an oxide surface localized chemical bonds are formed. The chemisorbed species and the region of the oxide substrate directly participating in the chemical bond will have an electronic structure similar to that of a $\text{MO}_6\text{-C}$ or $\text{MO}_5\text{-C}$ complex (C is the chemisorbed species). In addition there are many transition-metal oxides for which the d electrons are localized and do not form bands. In such cases a cluster model is more appropriate than a one-electron band model. It is also of interest to consider how the states of the MO_6 cluster are related to the energy bands of the corresponding solid in order to assess the validity of using cluster results to interpret electronic and optical properties of d -band perovskites. Finally, we note that chemisorption and catalysis on very small particles may approach a condition described by a cluster model.⁵

We wish to correlate the qualitative properties of a TiO_6 cluster with those of several titanium oxides, including TiO_2 , SrTiO_3 , and BaTiO_3 , for which each titanium ion is approximately in a +4 valence state and surrounded by an octahedron of oxygen ions. Also, one may include Ti_2O_3 , for which the valence state is approximately Ti^{+3} . In addition to the approximations obviously involved in using a cluster model several other approximations are used. In the case of TiO_2 or Ti_2O_3 we ignore the distortion of the octahedra from cubic symmetry. This approximation omits important optical and electronic anisotropies but the general features of the electronic structure should be valid.

In applying the MO_6 cluster model to the perovskites $SrTiO_3$ and $BaTiO_3$ (in the cubic phase) we ignore the electronic states associated with the Sr or Ba ions. Previous studies^{1,6} show that the major effect on the bands near the energy gap is through the electrostatic potentials of the Sr or Ba ion and that the s -like states of these ions produce bands far removed from the energy gap. If the Madelung potentials⁷ arising from Sr or Ba ions are included in a linear-combination-of-atomic-orbitals (LCAO) model excellent quantitative results are obtained for the p and d bands. We have previously shown^{1,2} that such a model produces results which are in excellent agreement with the augmented-plane-wave (APW) results of Mattheiss⁸ and which also explains much of the structure in the optical properties observed by Cardona.⁹ With these approximations the electronic structure of clusters representing TiO_2 , $SrTiO_3$, and $BaTiO_3$ differ only in a minor way owing to small differences in Madelung potentials.

II. QUALITATIVE FEATURES OF THE MO_6 CLUSTER

The physical structure of the MO_6 cluster and a corresponding cubic perovskite is illustrated in Fig. 1. We describe first a simple model from which the essential features of the electronic structure of the MO_6 cluster can easily be understood and related to energy-band states. The cluster states may be discussed using atomiclike basis states corresponding to the $3d$ and $4s$ states of the cation and the $2p$ states of the oxygen ions.¹⁰ (A more general model including $2s$ oxygen states and $4p$ cation states used in the numerical calculations is described in Sec. IV.) The cluster wave functions and energies are easily derived in terms of two-center overlap and transfer integrals¹¹ as presented in Table I. The first column lists the cluster-state designations and symmetry. The second column gives the equivalent energy-band symmetry. The third through fifth columns give the degeneracy, total number of states, and the basis orbitals involved, respectively. The notation $2p_\sigma$ and $2p_\pi$ refers to p orbitals centered on an oxygen with lobes respectively parallel and perpendicular to the M -O axis. The energy of a particular cluster state is given by E^\pm , with the function A calculated using the appropriate E_1 , E_2 , S_1 , S_2 , and t parameters listed in columns six through ten. The plus sign of E^\pm corresponds to the upper cluster state. The energies of the t_{1g} and t_{2g} states are given directly in Table I. The energies E_{4s} , E_e , E_t , E_0 , and E_π are diagonal LCAO matrix elements roughly equal to the appropriate ionization or affinity energy but including Madelung and multipole electrostatic potentials in a manner de-

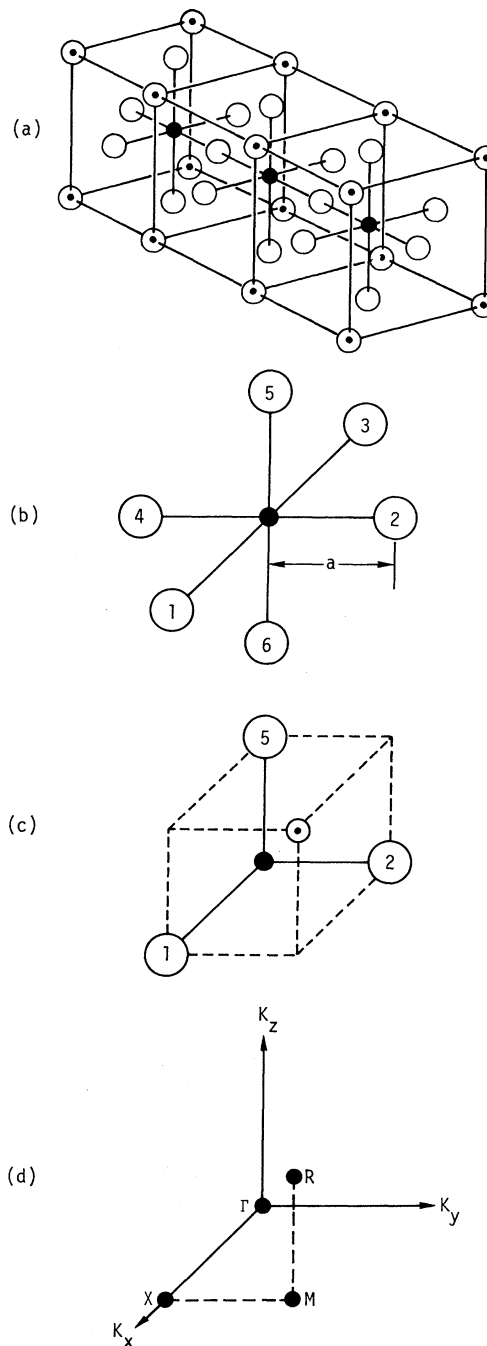


FIG. 1. (a) AMO_3 perovskite structure (the A ions are indicated by \odot and M ions by \bullet); (b) MO_6 cluster; (c) unit cell for AMO_3 perovskite; (d) Brillouin zone for the perovskite structure.

scribed previously.¹ The relevant two-center transfer and overlap integrals defined in the usual manner¹¹ are listed in the bottom of Table I. The symbol S is used to denote an overlap integral. The corresponding normalized LCAO wave-func-

TABLE I. Parameters for determining the MO₆ cluster and band energies according to the LCAO model.

Cluster state	Band Symmetry	Degeneracy	Total states	Basis	Cluster states			Band states						
					E ₁	E ₂	S ₁ S ₂	E ₁	E ₂	S ₁ S ₂	t			
7a _{1g} 6a _{1g}	R	1	2	4s, 2p _σ	E _{4s}	E _σ - 4a	4S _u	√6 S _g p _σ	√6 (spσ)	E _{4s}	E _σ - 8a	8S _u	√12 S _g p _σ	√12 (spσ)
3e _g 2e _g	R	2	4	d _{z²} , 2p _σ	E _e	E _σ + 2a	-2S _u	√3 S _g d _σ	√3 (pdσ)	E _e	E _σ + 4a	-4S _u	√6 S _g d _σ	√6 (pdσ)
2t _{2g} 1t _{2g}	R	3	6	d _{xy} , 2p _π	E _t	E _π - 2a	2S _u	2S _g d _π	2 (pdπ)	E _t	E _π - 4a	4S _u	2√2 S _g d _π	2√2 (pdπ)
6t _{1u} 5t _{1u}	Γ	3	6	2p _σ , 2p _π	E _σ	E _π + 2b	-2S _g	-2√2 (S _u + S _g)	-2√2 (a + b)	E _σ	E _π + 4b	-4S _g	-4√2 (S _u + S _g)	-4√2 (a + b)
1t _{1g}	R	3	3	2p _π				E = (E _π + 2a)/(1 + 2S _u)					E = (E _π + 4a)/(1 + 4S _u)	
1t _{2u}	Γ	3	3	2p _π				E = (E _π - 2b)/(1 - 2S _g)					E = (E _π - 4b)/(1 - 4S _g)	

$$E^{\pm} = A \pm \left(A^2 + \frac{E_1(1-S_1) + E_2 - 2E_2}{1-S_1 - S_1^2} \right)^{1/2}, \quad A = \frac{1}{2} [(2p, 2p, \sigma) - (2p, 2p, \pi)], \quad (pd\sigma) = (2p, 3d, \sigma), \quad (sp\sigma) = (4s, 2p)$$

$$S_u = \frac{1}{2} [S(2p, 2p, \sigma) - S(2p, 2p, \pi)], \quad S_b = S(2p, 3d, \sigma), \quad S_{p\pi} = S(2p, 3d, \pi), \quad S_{g\sigma} = S(4s, 2p, \sigma)$$

tions ψ^{\pm} may be obtained from Table II using the parameters and energies from Table I. In Table II the notations x_{α} , y_{α} , and z_{α} are used to denote p orbitals on the α th oxygen ion as designated in Fig. 1(b).

A schematic of typical cluster energies is given by Fig. 2(a). From Tables I and II the nature of the cluster states is evident. The t_{1g} , t_{2u} , and t_{1u} states are "nonbonding" since they do not involve hybridization with the M -ion orbitals. One interesting result is that the energy difference between the $1t_{1g}$ and $1t_{2u}$, a direct measure of the oxygen-oxygen interaction, is independent of the M ion. This result is generally valid for LCAO basis and is unaffected by the addition of $4p$ and $2s$ basis functions. Thus for different oxides with the same M -O distance this energy difference should be constant. Self-consistent $X\alpha$ calculations for rutile, Wustite, and Hematite¹² and also for nickel oxide⁵ appear to support this conclusion.

The cluster bonding states are the $2e_g$ and $1t_{2g}$ levels which involve an admixture of M -ion and oxygen orbitals. Typical oxides will have a 20 to 30% M -ion content in the bonding wave function.^{1,5,12} The t_{2g} d states (d_{xy} , d_{xz} , and d_{yz}) are mixed with the $2p_{\pi}$ orbitals by the $(2p, 3d, \pi)$ two-center interaction. The e_g d states are mixed with the $2p_{\sigma}$ orbitals by the $(2p, 3d, \sigma)$ interaction. The corresponding antibonding "crystal-field" states are the $3e_g$ and $2t_{2g}$ states. The a_{1g} cluster levels also involve hybridization of the M -ion and oxygen orbitals. The M -ion $4s$ states are mixed with the $2p_{\sigma}$ orbitals by the $(2p, 4s, \sigma)$ two-center integral.

In insulating perovskites such as SrTiO₃, BaTiO₃, or KTaO₃, or in TiO₂, the highest occupied state is the $1t_{1g}$ and the energy difference $E(2t_{2g}) - E(1t_{1g})$ corresponds approximately to the energy gap between the lower conduction band and the upper valence band. The $2t_{2g}$ may be partially occupied by reducing the material (in a hydrogen environment, for example) or by the application of light with $h\nu$ greater than the band-gap energy. In metallic perovskites such as³ KMoO₃ or¹³ ReO₃ the $2t_{2g}$ states are partially occupied. The energy difference $E(3e_g) - E(2t_{2g})$ is the crystal-field splitting $10Dq$.

III. CORRELATION OF CLUSTER STATES WITH BAND STATES

There is a strong correlation between the cluster states and the energy-band states of the corresponding solid at points of high symmetry in the Brillouin zone. The correspondence for the perovskites is particularly simple. The group of the k vector possesses full cubic symmetry (O_h) at the points Γ and R in the Brillouin zone. The cluster wave functions and energies can be directly

TABLE II. Wave functions for the MO_6 cluster.

Cluster type	ψ_1	Wave functions	ψ_2
a_{1g}	ϕ_{4s}	$\frac{1}{\sqrt{6}(1-S_1)^{1/2}}(-x_1-y_2+x_3+y_4-z_5+z_6)$	
e_g	$\phi_{x^2-y^2}$	$\frac{1}{2(1-S_1)^{1/2}}(-x_1+y_2+x_3-y_4)$	
t_{2g}	ϕ_{xy}	$\frac{1}{2(1-S_1)^{1/2}}(y_1+x_2-y_3-x_4)$	
t_{1u}	$\frac{1}{\sqrt{2}}(-x_1-x_3)$	$\frac{1}{2(1-S_1)^{1/2}}(x_2+x_4+x_5+x_6)$	
t_{1g}		$\frac{1}{2(1+2S_2)^{1/2}}(y_1-x_2-y_3+x_4)$	
t_{2u}		$\frac{1}{2(1-2S_2)^{1/2}}(x_2+x_4-x_5-x_6)$	
$\psi^\pm = \frac{(t-E^\pm S_2)(1-S_1)^{1/2}\psi_1 - (E_1-E^\pm)\psi_2}{[(t-E^\pm S_2)^2(1-S_1) + (E_1-E^\pm)^2 - 2(t-E^\pm S_2)(E_1-E^\pm)S_2]^{1/2}}$			

related to the energy-band wave functions and energies at either Γ or R . The appropriate band symmetry is listed in Table I, column two. An LCAO tight-binding model including first- and second-neighbor interactions yields energies which may be calculated from Table I using E^\pm and the parameters listed in columns 11–15. The E_1 , E_2 , S_1 , S_2 , and t parameters entering the calculations for the band states differ from the cluster-state parameters only in the numerical coefficients. Cluster state's two-center transfer and overlap integrals are smaller than band state's by a factor of $\sqrt{2}$ for M -ion-oxygen interactions and a factor of 2 for oxygen-oxygen interactions. These increase in the transfer and overlap interactions reflect the fact that each oxygen is shared by two octahedra in the solid. Because of the way that the LCAO parameters enter the expressions for the energies, there is no simple relation between the energy of a cluster level and the "center of gravity" of the corresponding energy band.

The relationship between cluster and band states is clearer if the wave functions are considered. For example, the energy-band wave function at Γ corresponding to a cluster state may be calculated using Table II to obtain the cluster state and then repeating the cluster wave function in every unit cell. The same procedure applies to band states at R except that the phase of the wave function is reversed in adjacent unit cells. This is illustrated in Fig. 3 for the $1t_{1g}$ state and corresponding band state at R .

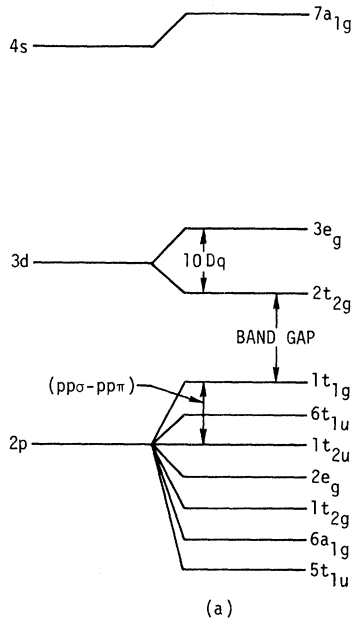
A schematic of the energy bands of a typical d -band perovskite is shown in Fig. 2(b). The mix-

ing of the t_{2g} d orbitals with the $2p_\pi$ orbitals through the $(2p, 3d, \pi)$ two-center interaction produces the $pd\pi$ valence band and the $pd\pi^*$ conduction band. The e_g d orbitals interact with the $2p_\sigma$ orbitals to produce the $pd\sigma$ and $pd\sigma^*$ valence and conduction bands. The oxygen-oxygen interactions ($pp\sigma$ and $pp\pi$) produce further splittings and add to the band widths of both π and σ bands. The corresponding cluster symmetries are indicated in Fig. 2(b). The ordering of the cluster and band levels depends upon the relative magnitudes of the LCAO parameters and therefore on the particular cluster being considered.

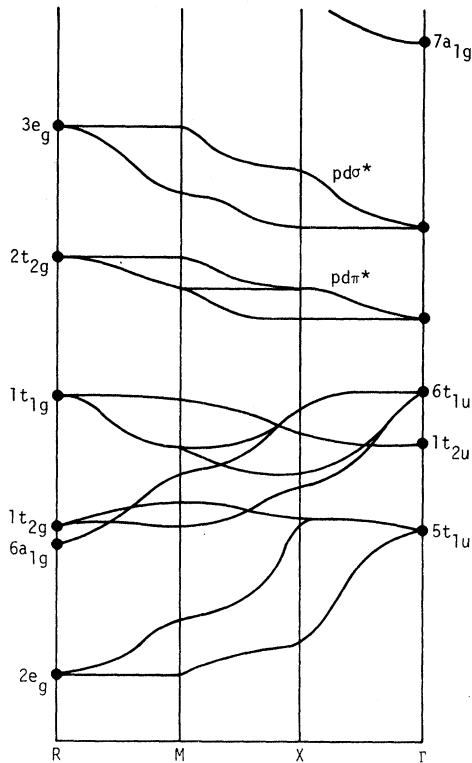
The model discussed in this section leads to an exact one-to-one correspondence between cluster levels and band states at *either* Γ or R . The addition of $4p$ M -ion basis states does not alter this correspondence but when $2s$ oxygen orbitals are included the exact correspondence is lost. In this more general case the cluster states a_{1g} , e_g , and t_{1u} would have projections onto both Γ and R band states. The mixing is very small, however, because the diagonal energy of the $2s$ states^{8,12} is far removed from that of the $2p$ or $3d$ states. Thus the analysis presented above remains valid even though it is not exact.

IV. TiO_6 CLUSTER

LCAO calculations were made using 33 basis functions representing $3d$, $4s$, and $4p$ M -ion orbitals and $2p$ and $2s$ orbitals for each of the six oxygen atoms. The two-center overlap and transfer integrals were determined by fitting the



(a)



(b)

FIG. 2. Schematic of MO_6 cluster states and energy bands of a perovskite. (a) Cluster states. The crystal-field splitting $10Dq$ and the band gap are indicated. The difference between the $1t_{1g}$ and $1t_{2u}$ nonbonding levels is a direct measure of the oxygen-oxygen interaction ($pp\sigma-pp\pi$). (b) Perovskite energy bands. States with cluster symmetries are labeled at Γ and R .

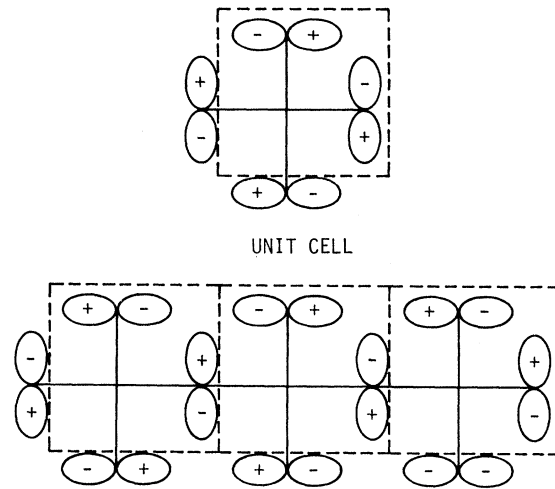


FIG. 3. Schematic of the $1t_{1g}$ cluster state and the corresponding band state at R in the Brillouin zone.

energies of the cluster states for rutile as determined by Tossel, Vaughan, and Johnson,¹² who used a self-consistent $X\alpha$ method. The overlap parameters were found to be small, in agreement with the results deduced by Mattheiss⁸ based on APW calculations for SrTiO_3 . Therefore to reduce the number of parameters in our model, overlap effects were discarded and orthogonal basis states were assumed. The cluster states of TiO_6 shown in Fig. 4(b) were obtained using the two-center parameters indicated in Table III. The solid dots in Fig. 4(b) indicate the results of Tossel, Vaughan and Johnson.¹²

In addition to the states discussed in Sec. III new states appear because of the added $4p$ and $2s$ basis states. The group $5a_{1g}$, $1e_g$, and $4t_{1u}$ are essentially oxygen $2s$ states and the $7t_{1u}$ level is derived from the $4p$ M -ion states. The $4p$ states also enter into the $5t_{1u}$ and $6t_{1u}$ levels so that these levels are no longer nonbonding. The diagonal energies E_{4s} , E_e , E_t , E_σ , and E_π include the effects of the electrostatic potentials due to all of the charged ions that would be present in BaTiO_3 , and SrTiO_3 in a manner discussed previously.¹ The potentials for pseudocubic TiO_2 are essentially the same as those for the perovskites and no distinction is made in the calculations presented here.

The LCAO parameters derived by Mattheiss⁸ for SrTiO_3 are also presented in Table III for comparison (numbers in parentheses). To fix the absolute energy scale for Mattheiss's diagonal matrix elements, E_t was chosen to be 5.4 eV and E_e was deduced from Mattheiss's parameter E_d

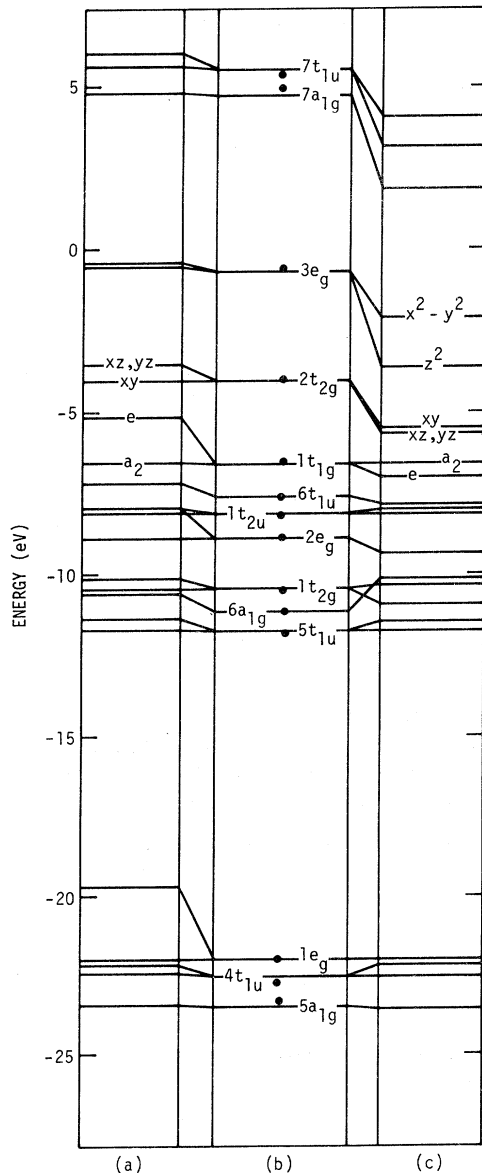


FIG. 4. Cluster bulk and surface states. (a) TiO_6 surface cluster, (b) TiO_6 bulk cluster, (c) TiO_5 surface cluster.

using his value of 2.4 eV for the d -state electrostatic splitting at Γ . Parameters corresponding to the $4s$ and $4p$ states were not given by Mattheiss. It is seen from Table III that there is reasonable agreement for all the parameters listed with the exception of the parameter $(2p, 2p, \sigma)$. The value of 1.4 eV deduced from the $X\alpha$ calculations is much larger than Mattheiss's value of 0.32 eV or that reported by Switendek¹⁴ of 0.38 eV. The

large value of $(2p, 2p, \sigma)$ is a direct result of the large separation of the $1t_{1g}$ and $1t_{2u}$ cluster states and it is not possible to fit these levels with a smaller value of the parameter. This discrepancy is very serious. The use of a value of $(2p, 2p, \sigma)$ as large as 1.4 eV in any tight-binding energy-band model for TiO_2 or for SrTiO_3 would cause valence bands to rise *above* the lower conduction bands at and near Γ and thus a metallic state would be predicted. Therefore, in a band model a smaller value of $(2p, 2p, \sigma)$ must be employed.

V. CLUSTER SURFACE STATES

The surface energy bands of d -band perovskites have been discussed in a previous paper.^{1,3} It was shown that a high density of surface states (involving the t_{2g} d states) derived from the $pd\pi^*$ bands would occur in the energy gap. Surface energy bands derived from the $pd\sigma^*$ bands can also occur. The surface bands arise because of a variety of effects at a solid surface, including missing neighboring atoms, changes in the Madelung potentials, loss of symmetry and accompanying changes in the crystalline field, changes in the separations between atomic layers at and near the surface, and reconstruction of the surface layer. In the work described here we include the effects of missing atoms and the variations of the Madelung potentials at or near the surface.

There are two types of (001) surface configurations for the perovskite structure.¹ For the type-I surface, M ions and oxygen ions are exposed on the surface layer, while for the type-II (001) surface the M ions are buried in the second atomic layer.

The repulsive Madelung potential at a Ti ion on a type-I surface of SrTiO_3 or BaTiO_3 is reduced by 2 eV from the bulk potential.^{1,3} The Madelung potential at a surface oxygen site, however, is essentially the same as in the bulk. The cluster analog of the type-I perovskite surface consists of a TiO_5 cluster with the Madelung potential acting on the Ti ion reduced by 2 eV.

On a type-II surface of the perovskite the Madelung potential acting on a surface oxygen is reduced by 2.9 eV while that of the Ti ion in the second layer is essentially unchanged from the bulk value.^{1,3} The cluster analog of the type-II perovskite surface consists of a TiO_6 cluster with the Madelung potential acting on *one* of the oxygens reduced by 2.9 eV.

In the case of both the TiO_5 and TiO_6 surface analogs the point-group symmetry is C_{4v} rather than O_h . Group-theoretical analysis¹⁵ shows that the irreducible representations of O_h split into those of C_{4v} as follows:

TABLE III. LCAO parameters for the TiO_6 cluster. Columns two and five are parameters determined in the present study. Columns three and six are parameters reported by Mattheiss for SrTiO_3 (see Ref. 13).

Parameter	Value in eV (Mattheiss)		Parameter	Value in eV (Mattheiss)	
E_e	-2.84	(-3.0)	$(2p, 2p, \pi)$	-0.1	(-0.1)
E_t	-5.4	(-5.4)	$(2p, 4p, \sigma)$	4.6	...
E_σ	-8.7	(-8.3)	$(2p, 4p, \pi)$	-0.9	...
E_π	-8.0	(-8.5)	$(2p, 4s, \sigma)$	-0.8	...
E_{2s}	-21.0	(-23.2)	$(2p, 2s, \sigma)$	-0.1	(0.0)
E_{4s}	-0.8	...	$(2s, 2s, \sigma)$	-0.3	(-0.133)
E_{4p}	-1.0	...	$(2s, 4s, \sigma)$	-3.9	...
$(2p, 3d, \sigma)$	-1.9	(-2.04)	$(2s, 3d, \sigma)$	-1.7	(-2.56)
$(2p, 3d, \pi)$	1.3	(1.14)	$(2s, 4p, \sigma)$	-3.95	...
$(2p, 2p, \sigma)$	1.4	(0.3)	$S(2p, 3d, \sigma)$	0.0	(0.078)
$S(2s, 3d, \sigma)$	0.0	(0.043)	$S(2s, 3d, \pi)$	0.0	(-0.058)

$$\begin{aligned}
 a_{1g} \rightarrow a_1, \quad e_g \rightarrow a_1 + b_1, \quad t_{1g} \rightarrow a_2 + e, \\
 t_{1u} \rightarrow a_1 + e, \quad t_{2g} \rightarrow b_2 + e, \quad t_{2u} \rightarrow b_1 + e.
 \end{aligned}
 \quad (1)$$

The e representation is two-dimensional and all others of the C_{4v} group are one-dimensional. The decomposition of the regular representations Γ_R (the representation in terms of the $2p$, $2s$, $3d$, $4s$, and $4p$ basis functions) is

$$\Gamma_R(\text{TiO}_6) = 10a_1 + a_2 + 4b_1 + 2b_2 + 8e, \quad (2)$$

$$\Gamma_R(\text{TiO}_5) = 8a_1 + a_2 + 4b_1 + 2b_2 + 7e. \quad (3)$$

The difference between $\Gamma_R(\text{TiO}_6)$ and $\Gamma_R(\text{TiO}_5)$ of $2a_1$ and e accounts for the loss of three $2p$ and one $2s$ states associated with the missing oxygen in TiO_5 .

The LCAO model described in Sec. IV was used to calculate new cluster states which are the analogs of surface bands. The results for the TiO_5 cluster are shown in Fig. 4(c). These states were obtained using the parameters of Table III with the Ti-ion diagonal energies E_{4s} , E_{4p} , E_t , and E_e reduced by 2.0 eV.

For the discussion here the important cluster surface states are those derived from the $2t_{2g}$ and $3e_g$ states labeled xy , xz , yz and $x^2 - y^2$ and z^2 in Fig. 4(c). These labels designate the primary orbitals involved. The xy and xz , yz surface states correspond respectively to b_2 and e symmetry, as indicated in Eq. (1). The $x^2 - y^2$ and z^2 surface states correspond to a_1 and b_1 symmetry.

The group of the k vector at the point M in the Brillouin zone is C_{4v} and consequently these cluster

surface states should be compared to surface band states at M . The bulk and surface bands for SrTiO_3 or BaTiO_3 are shown in Fig. 5 together with the relevant cluster surface states. These

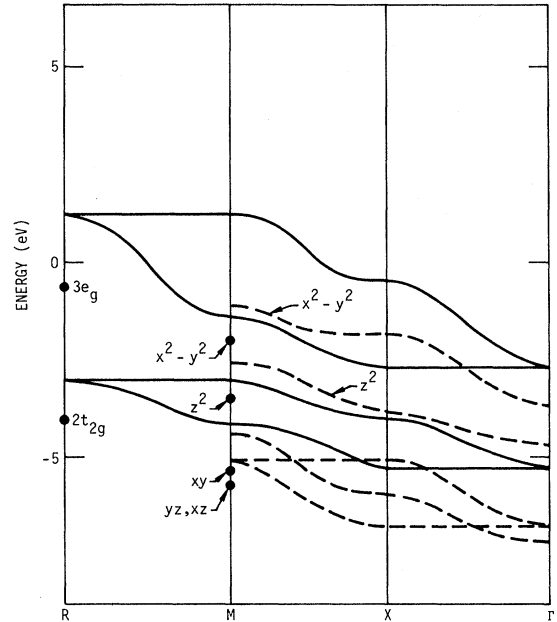


FIG. 5. d -electron conduction bands of SrTiO_3 . The solid curves are the bulk conduction bands. The dashed curves are the surface-state energy bands for a (001) type-I surface. The corresponding TiO_6 bulk states are indicated by dots at R in the Brillouin zone. The TiO_5 cluster surface states are indicated by dots at M in the Brillouin zone.

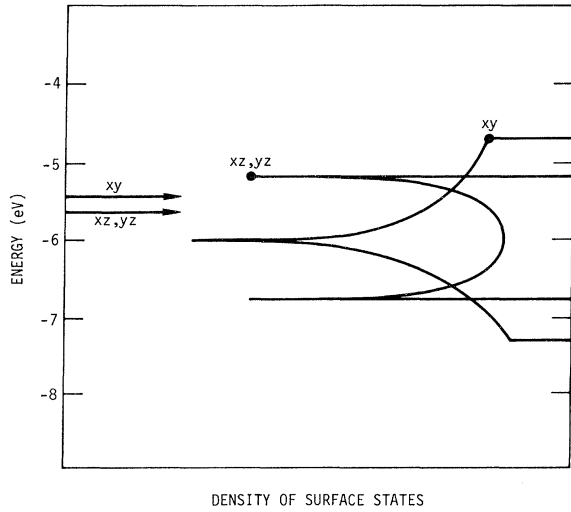


FIG. 6. Schematic of the surface density of states for SrTiO_3 . The solid curves are the surface energy bands. The dots indicate the energy at M in the Brillouin zone. The corresponding surface-cluster-state energies of TiO_6 are indicated by arrows.

band states were calculated using the same parameters employed in the cluster calculation, except that Mattheiss's value for $(2p, 2p, \sigma)$ was adopted. The method of calculation was discussed in a previous paper.¹

The $pd\sigma^*$ surface bands corresponding to $x^2 - y^2$ and z^2 at M lie below the bulk states by 2.4 and 3.8 eV. The corresponding cluster surface states are 1.5 and 3.1 eV below their parent states in TiO_6 . It should be mentioned that the $x^2 - y^2$ surface band is a virtual surface band when it lies within the bulk continuum of $pd\sigma^*$ states. The $pd\pi^*$ surface bands corresponding to xy and xz, yz at M lie 0.5 and 1.3 eV below the bulk band. The corresponding surface cluster states lie 1.5 and 1.7 eV below their parent TiO_6 states. The highest filled valence state, a_2 , in Fig. 4(c) is essentially unchanged from the bulk $1t_{1g}$ level, in agreement with the band model,⁷ which shows no valence surface states in the gap for a type-I surface.

The results for the type-II surface corresponding to a TiO_6 cluster are shown in Fig. 4(a). These results were obtained from the LCAO model using the parameters of Table III with E_{2s} , E_{σ} , and E_{π} for one of the oxygen ions increased by 2.9 eV. The a_2 cluster surface state is raised into the gap between the $2t_{2g}$ and $1t_{1g}$ levels. The xy state is essentially unchanged in energy from the $2t_{2g}$ state. These results are in agreement with the band model,¹ which shows no conduction-band surface states in the energy gap for a type-II sur-

face subject to the same surface perturbation used for the cluster. The differences in cluster energies compared to band energies can be understood from the fact that oxygen ions are shared by two octahedra in the solid but not in the cluster.

A schematic of the surface energy-band densities of states^{2,3} is given in Fig. 6. The xy -band density possesses sharp discontinuities at the band edges and a logarithmic singularity at the center of the band. These Van Hove singularities are characteristic of two-dimensional energy bands and are also possessed by the bulk bands. Experimental evidence for the existence of this structure has been discussed in a previous paper.² The xz and yz bands produce a density of states with square-root singularities at the band edges. These Van Hove singularities are characteristic of one-dimensional energy bands as discussed in our previous work.³ The location of the corresponding cluster-surface-states energies is also shown in Fig. 6.

VI. DISCUSSION

In the preceding sections we examined the relation between MO_6 cluster-state energies and wave functions and those of energy-band states of a perovskite at Γ or R in the Brillouin zone. The cluster analog surface states were also presented and correlated with surface band states occurring at M in the Brillouin zone. The cluster model is seen to represent in a qualitative manner many of the electronic features of the corresponding solid. In this section we present brief discussions of these results.

The electronic structure of TiO_2 and Ti_2O_3 surfaces has been studied recently by Henrich, Dresselhaus, and Zeiger¹⁶ using electron energy-loss spectroscopy. They observe a large peak at 1.5–2 eV in the electron energy-loss spectrum of freshly broken samples of Ti_2O_3 but not for TiO_2 . After sputter etching with Ar ions the TiO_2 samples also exhibited the 2-eV peak. Subsequent exposure to oxygen removed the peak in TiO_2 and diminished the intensity in Ti_2O_3 . Based on Auger studies, the sputter etching by Ar ions was believed to reduce the surface.

Henrich, Dresselhaus, and Zeiger suggest that the 2-eV peak may be associated with $\text{Ti}^{+3}(3d^1)$ surface ions on Ti_2O_3 or created on TiO_2 by the sputter-etching process. The 2-eV energy is then attributed to transitions between the crystal-field-split levels of the $3d^1$ states of Ti^{+3} ions.

We suggest that the transitions between crystal-field surface states, $xz - z^2$, may be involved. According to cluster calculations $10Dq \approx 3-3.5$ eV; however, as illustrated in Fig. 4(c), the splitting of the d -electron states of a TiO_6 cluster (E_{xz}

$-E_g$) is reduced to about 2.0 eV. The band model gives the same result. These levels would be replaced by crystal-field states separated by about 3 eV when oxidation occurs converting TiO_5 to TiO_6 [see Fig. 4(a)]. The band gap in TiO_2 is also about 3 eV and consequently crystal-field transitions in the TiO_6 surface cluster would be difficult to distinguish from band-gap transitions.

MO_6 cluster calculations have been frequently employed for the interpretation of the optical properties of oxides. For example, such models have been used recently to explain the optical properties of rutile, Wustite, and Hemite. In the case of materials such as rutile or perovskites for which energy-band formation occurs the use of cluster interpretations cannot be justified. It is clear from our discussion of the correspondence between cluster and band states that significant differences appear in the energies of corresponding states. These differences for titanium oxides range from 1 to 2 eV and are not uniform or unidirectional. In addition to energy differences, important density-of-states structure not represented by corresponding cluster states can produce peaks in the optical spectra which cannot be explained by the cluster model.

Consider the case of SrTiO_3 as illustrated by Fig. 2. The onset of interband optical absorption would be ascribed to transitions from the $1t_{1g}$ to the $2t_{2g}$ state according to the cluster model. In the band model transitions from states with these symmetries would occur at R in the Brillouin zone. However, it is well established that direct interband transitions along the line Γ to X determine the onset of optical absorption.^{2,8,9,17} The $1t_{1g} \rightarrow 2t_{2g}$ cluster transitions do not correspond in any way to these band transitions. Notice also that at Γ the highest occupied valence-band state has the symmetry of the $6t_{1u}$ cluster state and not $1t_{1g}$. Since there is no cluster analog of $pd\pi^*$ band states at Γ or X the cluster model omits the entire set of transitions which are responsible

for the optical absorption band edge. Another feature worth noting is that the band gap at R in the Brillouin zone corresponding to the cluster gap $2t_{2g} - 1t_{1g}$ is substantially larger than the minimum gap which occurs at Γ or X in cubic perovskites,^{1,8,9,17} and thus the energy for the onset of interband absorption will also be incorrect. Finally it is clear that oscillator strengths determined from cluster transitions will have no relation whatever to interband transitions intensities associated with band wave functions of symmetries not represented by cluster states.

The cluster surface model also offers a useful method for discussing the electronic structure of possible surface complexes which may be involved in chemisorption and catalysis on transition-metal oxides. We have employed the surface-state results in describing a possible mechanism for the dissociative chemisorption of molecular hydrogen on an oxide surface in which the final product is a pair of OH surface complexes. These results will be reported elsewhere.¹⁸

It is important to note that there are features of the surface energy bands that are not present in the cluster model. From Fig. 6 it is apparent that there are large density-of-states peaks not represented by corresponding cluster states. For example, the lower square-root singularity in the density of xz , yz surface states derives from nearly pure- d -electron surface states along the line Γ to X in Brillouin zone. There are no cluster analogs of these states. The central logarithmic singularity in the xy surface-state density derives from surface band states for which $\sin^2 k_x a + \sin^2 k_y a = 1$ (a is the M -O distance) which lie on a surface containing the X points in the Brillouin zone.^{1,2} There are no cluster states corresponding to this surface of the Brillouin zone. Thus significant density-of-states effects are omitted in the cluster model. In the application of a cluster model the implications of such omissions must be considered.

¹T. Wolfram, E. A. Kraut, and F. J. Morin, Phys. Rev. B **7**, 1677 (1973).

²T. Wolfram, Phys. Rev. Lett. **29**, 1383 (1972).

³F. J. Morin and T. Wolfram, Phys. Rev. Lett. **30**, 1214 (1973).

⁴T. Wolfram and F. J. Morin, Appl. Phys. **8**, 125 (1975).

⁵K. H. Johnson and R. P. Messmer, J. Vac. Sci. Technol. **11**, 236 (1974).

⁶A. H. Kahn and A. J. Leyendecker, Phys. Rev. **135**, A1321 (1964).

⁷E. A. Kraut, T. Wolfram, and W. F. Hall, Phys. Rev. B **6**, 1499 (1972).

⁸L. F. Mattheiss, Phys. Rev. B **6**, 4718 (1972); **6**, 4740 (1972).

⁹M. Cardona, Phys. Rev. **140**, A651 (1965).

¹⁰C. J. Ballhausen and H. B. Gray, *Molecular Orbital Theory* (Benjamin, New York, 1965).

¹¹J. C. Slater and G. F. Koster, Phys. Rev. **94**, 1498 (1954). Third-neighbor oxygen-oxygen interactions are omitted.

¹²J. A. Tossel, D. J. Vaughan, and K. H. Johnson, Am. Mineral. **59**, 319 (1974).

¹³L. F. Mattheiss, Phys. Rev. **181**, 987 (1969); Phys. Rev. B **2**, 3918 (1970).

¹⁴A. C. Switendick, Quarterly Progress Report No. 49, 1963, Solid State and Molecular Theory Group, MIT, Cambridge, Mass. (unpublished).

¹⁵E. P. Wigner, *Group Theory and Its Application to the Quantum Mechanics of Atomic Spectra* (Academic, New York, 1959).

¹⁶V. E. Henrich, G. Dresselhaus, and H. J. Zeiger, Thirty-Fifth Annual Conference on Physical Electronics, Pennsylvania State University, 1975 (unpublished).

¹⁷K. W. Blazey, Phys. Rev. Lett. 27, 146 (1971).

¹⁸F. J. Morin and T. Wolfram (unpublished).